Photochemistry and Photobiology, 2012, 88: 831–839

Eosin Y Triplet State as a Probe of Spatial Heterogeneity in Microcrystalline Cellulose

Hernán B. Rodríguez[1], Enrique San Román*[1], Paulo Duarte[2], Isabel Ferreira Machado[2] and Luis F. Vieira Ferreira*[2]

[1]INQUIMAE/DQIAyQF, Facultad de Ciencias Exactas y Naturales, UBA, Ciudad Universitaria, Buenos Aires, Argentina
[2]CQFM-Centro de Química-Física Molecular and Institute of Nanoscience and Nanotechnology, Instituto Superior Técnico, Universidade Técnica de Lisboa, Lisboa, Portugal

Received 31 December 2011, accepted 20 March 2012, DOI: 10.1111/j.1751-1097.2012.01152.x

ABSTRACT

The photophysical behavior of eosin Y adsorbed onto microcrystalline cellulose was evaluated by reflectance spectroscopy, steady-state fluorescence spectroscopy and laser induced time-resolved luminescence. On increasing the concentration of the dye, small changes in absorption spectra, fluorescence redshifts and fluorescence quenching are observed. Changes in absorption spectra point to the occurrence of weak exciton interactions among close-lying dye molecules, whereas fluorescence is affected by reabsorption and excitation energy trapping. Phosphorescence decays are concentration independent as a result of the negligible exciton interaction of dye pairs in the triplet state. Lifetime distribution and bilinear regression analyses of time-resolved phosphorescence and delayed fluorescence spectra reveal the existence of two different environments: long-lived, more energetic triplet states arise from dyes tightly entrapped within the cellulose chains, while short-lived, less-energetic states result from dyes in more flexible environments. Stronger hydrogen bond interactions between the dye and cellulose hydroxyl groups lead in the latter case to a lower triplet energy and faster radiationless decay. These effects, observed also at low temperatures, are similar to those encountered in several amorphous systems, but rather than being originated in changes in the environment during the triplet lifetime, they are ascribed in this case to spatial heterogeneity.

INTRODUCTION

Suitable dyes have been used as fluorescent or phosphorescent probes for the study of heterogeneity in a broad range of organic amorphous materials, such as carbohydrates (1), gelatin (2) and synthetic polymers (3,4). These materials exhibit generally static and dynamic heterogeneity: at a given time, photophysical properties are a function of local packing densities and interactions with the probe, whereas, at given sites, environment dynamics may lead to time-dependent changes on the excited state behavior. The observation of nonexponential relaxation processes of excited singlet and triplet states allows monitoring heterogeneity at different time scales. On the other hand, substrates bearing adsorbed, embedded or chemically linked dyes in the form of thin films, micro and nanoparticles have been considered for different practical purposes, mainly photosensitization of solar cells (5,6) and generation of singlet oxygen (7,8).

Low concentrations are used for environment sensing to avoid dye-to-dye interactions and studies are currently carried out as a function of temperature at a fixed concentration. In contrast, the development of photosensitizing devices requires large dye local concentrations to improve light absorption. In these conditions, molecular aggregates are currently formed. Exciton interactions among an excited singlet and the ground state partner in a dimer cause the splitting of singlet energy levels. Depending on the relative orientation of the monomers, the aggregate may act as energy trap reducing fluorescence quantum yields and, in some cases, triplet yields may be enhanced. The magnitude of the interaction depends on the proximity of the dyes (third-power law) and the transition moment of the radiative transition. As singlet-triplet transitions are forbidden, the interaction almost vanishes when a triplet dimer is formed (9). Even a random distribution of dye molecules noninteracting in the ground state can lead to the existence of close-lying dye pairs, which may undergo exciton interactions and act as statistical traps of the singlet excitation energy (10,11).

Xanthene dyes have been considered for the development of polymer based singlet oxygen photosensitizers (12) and to extend the response of photoelectrochemical cells to the visible region of the electromagnetic spectrum (13). Eosin Y is a xanthene dye broadly used in medicine, biology, the drug industry, cosmetics, textile dyeing and ink manufacturing, among other applications. It differs from fluorescein by the presence of four bromine atoms at positions 2, 4, 5 and 7 of the xanthene ring (see Scheme 1). Due to the presence of the bromine atoms attached to the xanthene skeleton and the consequent increase of the intersystem crossing rate, the photophysical properties of this dye differ significantly from those of other dyes composed exclusively of light atoms, namely rhodamine, oxazine, fluorescein or acridine, in which the triplet quantum yield, Φ_T, is usually small.

The photophysical properties of xanthene dyes are strongly dependent on the environment. On going from water to

*Corresponding authors email: esr@qi.fcen.uba.ar (Enrique San Román); luisfilipevf@ist.utl.pt (Luis Filipe Vieira Ferreira)

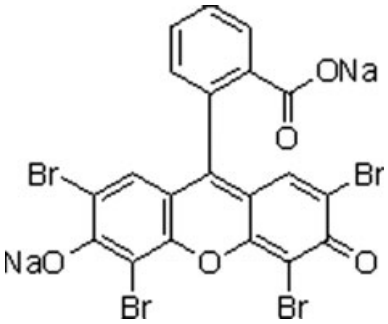

Scheme 1. Eosin Y.

alcohols fluorescence quantum yields increase at the expense of intersystem crossing (14). The dianionic salt of eosin Y has a moderate to high triplet quantum yield, Φ_T = 0.18–0.56 in methanol and 0.4–0.8 in water (most values are estimations; 15). The fluorescence quantum yield has been determined in ethanol as Φ_F = 0.67 (16), whereas Φ_F values of 0.15–0.22 in water, 0.44–0.63 in methanol and 0.40–0.69 in ethanol have been found (17). The same source cites Φ_T = 0.33–0.43 in ethanol. Recently, Penzkofer *et al*. reported on the photophysics of eosin Y in the millimolar concentration range in micrometer sized films of gelatin, starch and chitosan (18). Comparison of delayed fluorescence with phosphorescence quantum yields allowed estimation of Φ_T under certain assumptions; values around 0.2 were obtained. Phosphorescence and delayed fluorescence decays are nonexponential with a long-term lifetime around 4 ms. A faster component was attributed to quenching by dissolved molecular oxygen.

Xanthene dyes have been used to monitor molecular mobility and site heterogeneity in different amorphous materials. In particular, Pravinata *et al*. studied molecular mobility in amorphous sucrose by steady-state and time-resolved phosphorescence of erythrosin B, a dye with the same structure as eosin Y with iodine instead of bromine atoms, between 5 and 100°C (19). Another extensively studied solid support is microcrystalline cellulose. Adsorbed species are immobilized in the rigid cellulose matrix by hydrogen bonding between the hydroxyl groups of the polymer chain and the guest molecule, reducing the molecular motion and increasing the adsorbate emission lifetime and quantum yield as reported in many cases. It was also reported that dyes adsorbed on cellulose are protected from quenching by molecular oxygen, as the mobility of this species is highly reduced in this medium, provided cellulose is well dried (20). In this way, interference from oxygen is easily avoided. Small amounts of water, however, strongly affect the excited state behavior of the adsorbed molecule (21). Some studies of xanthene and other dyes adsorbed on microcrystalline cellulose, such as rhodamine 6G, rhodamine 101, auramine O, rose bengal, etc., have been reported by us (10,22–24).

Studies of native or fibrous cellulose have shown that this medium acts as a two-phase system consisting of a less ordered and compact amorphous region, located mainly on the surface of the elementary fibrils, and well-ordered regions (crystallites), where cellulose chains exist in a definite crystal pattern. In the latter case, cellulose chains are aligned in a parallel fashion and closely packed together providing maximum hydrogen bonding between adjacent cellulose chains. Depending on the solvent swelling capacity both environments may be available: dye molecules may be entrapped and rigidly attached between cellulose polymer chains or adsorbed on the surface of crystallites, in a less rigid situation (22).

In this study, the absorption and luminescence properties of eosin Y adsorbed onto microcrystalline cellulose are studied. The photophysical behavior of the dye is evaluated by reflectance spectroscopy, steady-state luminescence and laser induced time-resolved luminescence, to characterize the state of the dye and the effects of dye-to-dye and dye-to-support interactions on its photophysical properties. A systematic study of the dependence of phosphorescence and delayed fluorescence spectra and decays with the concentration of the dye is performed. Lifetime distribution and bilinear analyses are employed together with experiments at low temperature as a means to discriminate among cellulose binding sites and test for static and dynamic heterogeneity.

MATERIALS AND METHODS

Chemicals and preparation of samples. Eosin Y disodium salt (EO) was obtained from Sigma–Aldrich and used as received. Dye purity (90%) was checked by absorption spectroscopy. Microcrystalline cellulose powder (pH 5–7, average particle size 20 μm) from Aldrich was dried in a vacuum oven at 40°C for 48 h before preparing the samples. Ethanol Biopack (analytical grade) was used without further purification. Solid samples were prepared by evaporation of the solvent from suspensions of weighed amounts of cellulose in ethanol solutions of the dye. The solvent was evaporated immediately after the preparation in a rotary evaporator at 40°C during ca 20 min. Samples were further dried in a vacuum at 40°C for 48 h. The same drying procedure was carried out before performing measurements. Samples with concentrations spanning two orders of magnitude were prepared: 0.0424; 0.0901; 0.159; 0.318; 0.636; 1.33; 2.65 and 4.24 μmol dye per gram cellulose (samples EO1–EO8, respectively).

Ground state diffuse reflectance absorption studies. Diffuse reflectance spectra were determined for optically thick samples (no light transmitted, 2–3 mm thick samples assure optical thickness) using an OLIS 14-VIS-NIR spectroscopy operating system with a diffuse reflectance attachment (90 mm diameter integrating sphere, internally coated with MgO). This apparatus has been modified to extend the initial operational range in the UV and visible region by installing a new detector (Hamamatsu R955, with spectral response in the 160–950 nm range) and including the possibility of using short-wavelength-pass filters to prevent the fluorescence of the dyes from reaching the detector. In this case, we used a Comar 610 GK 50 filter (22). MgO was used as a reference to adjust the 100% reflectance level. Remission (Kubelka–Munk) functions were obtained as $F(R) = (1 - R)^2/2R$, where R is the diffuse reflectance of the sample (25).

Steady-state fluorescence. Steady-state emission spectra were obtained in front face on a PTI Model QM-1 spectrofluorometer (Photon Technology International, London, Ontario, Canada). Emission spectra of optically thick and thin layers of particles were recorded to evaluate the effect of luminescence reabsorption. Thin layers were prepared spreading small amounts of powder on one side of a two-sided sticky tape fixed on a glass plate. The emission beam was passed through a suitable filter (Schott OG530, Schott AG, Mainz, Germany; 2 mm thickness) to avoid excitation reaching the detector. Spectra were corrected for changes in the detector responsivity and filter transmittance with wavelength.

Fluorescence quantum yields. The determination of fluorescence quantum yields of dyes adsorbed on powdered solids is more difficult than the equivalent experiment in liquids, as it involves evaluation of the remission function of the dye and fluorescence reabsorption effects become significant. This affects both the fluorescence emission intensity and the shape of the spectra (26,27).

For strongly fluorescent solid samples, reflectance is overestimated by luminescence reaching the photodetector. Observed fluorescence quantum yields can be calculated from reflectance spectra with and without filter in front of the detector and considering thick layer emission spectra corrected for changes in the detector responsivity with

wavelength (28,29). Absolute fluorescence quantum yields were calculated from total reflectance measurements with and without a suitable filter (Schott BG38, 2 mm thickness), which cuts a substantial amount of the emission of the solid sample. Measurements were performed on a Shimadzu UV-3101 scanning spectrophotometer (Shimadzu Corporation, Kyoto, Japan) equipped with an integrating sphere, using barium sulfate as reference.

Laser induced luminescence. A description of the laser induced luminescence (LIL) system was presented recently in ref. (30). For the laser induced luminescence experiments, a N_2 laser (PTI model 2000, *ca* 600 ps FWHM, *ca* 1.0 mJ per pulse) and a reflection geometry mode were employed. The light arising from the solid powdered samples after excitation by the laser pulse was collected by a collimating beam probe coupled to a fused silica optical fiber and detected by a gated intensified charge coupled device (Andor Technology Limited, i-Star 720, model DH 720-18-F-03, Belfast, Ireland). The ICCD was coupled to a fixed imaging compact spectrograph (Shemrock 163). The system could be used either by capturing all light emitted by the sample (as in steady-state fluorescence spectra) or in time-resolved mode by the use of the internal delay capability of the i-Star 720. The ICCD has high-speed gating electronics (2.3 ns) and intensifier and covers the 200–950 nm wavelength range. Time-resolved emission spectra are available in the nanosecond to second time range both in transmission or diffuse reflectance modes.

Spectral and decay analyses were performed using tools developed in our laboratories. Lifetime distribution analysis (LDA) allows for asymmetric lifetime distributions using pseudo-Voigt (Gaussian and Lorentzian mixture) instead of pure Gaussian or Lorentzian profiles and is programed into the frame of Microsoft Excel Solver (31). This is a very convenient way to treat emission or transient absorption decay data because it reflects the multiplicity of sites available for the probe onto the specific surface under study. The model assumes that the lifetime distribution of an excited probe adsorbed on a heterogeneous, porous substrate is a consequence of a distribution of adsorption free energies around a mean value. It allows obtaining a distribution of lifetimes, α, whose rigorous definition can be found elsewhere (31). On the other hand, bilinear analysis allows factoring complex spectra into individual components. In the case under study time-resolved spectra are expressed in matricial form, each matrix element representing the phosphorescence intensity at a defined wavelength and time. The problem consists in finding a spectrum matrix (a column for each individual component) and a decay matrix (a row for each individual component), whose product is the matrix of time-resolved spectra. Every linear combination of rows (columns) in the spectrum (decay) matrix is a possible solution yielding a different decay (spectrum) matrix. Additional information allows finding the right combination. The method also permits the determination of the minimum number of individual components (32).

Diffuse reflectance laser flash photolysis. This technique was developed by Wilkinson and Kelly (33) by the end of the 80s. A schematic diagram of the diffuse reflectance laser flash photolysis (DRLFP) system was presented in ref. (34). Laser flash photolysis experiments were carried out with the fourth harmonic of a Nd:YAG laser (266 nm, *ca* 6 ns FWHM, 10–30 mJ per pulse) from B. M. Industries (Thomson-CSF, model Saga 12-10), in the diffuse reflectance mode. The detection system is the same as in LIL experiments, except for the monitoring light, which is used in this case (Xenon Lamp from Muller Electronic Optics, 450 W). Time-resolved absorption spectra are available in a time range from nanoseconds to seconds. Transient absorption data are reported as percentage of absorption, defined as $100\,\Delta J_t/J_o = 100(1 - J_t/J_o)$, where J_o and J_t are diffuse reflected light from sample before exposure to the exciting laser pulse and at time t after excitation, respectively.

RESULTS AND DISCUSSION

Ground state absorption

Figure 1 shows normalized remission function spectra of samples EO1–EO8, to which the cellulose background has been subtracted. The maximum (531 nm) is redshifted from the absorption in basic ethanol (525 nm; 16). The shoulder at 500 nm grows slightly with concentration. Absorption is rather low at wavelengths below 450 nm. The absorption of the supporting matrix (not shown in the figure) is quite broad (300–600 nm) and negligible compared with the visible absorption of the dye, but very important below 400 nm. The inset shows a representation of $F(R)$ at 531 nm as a function of the concentration of the dye. The linear fit with zero intercept (excluding sample EO7) is also shown. The linearity of the graph points to a small tendency of the dye to aggregate. However, the growing absorption of the shoulder relative to the maximum as dye concentration increases reflects the existence of weak exciton interactions among monomeric dye molecules located at short distances.

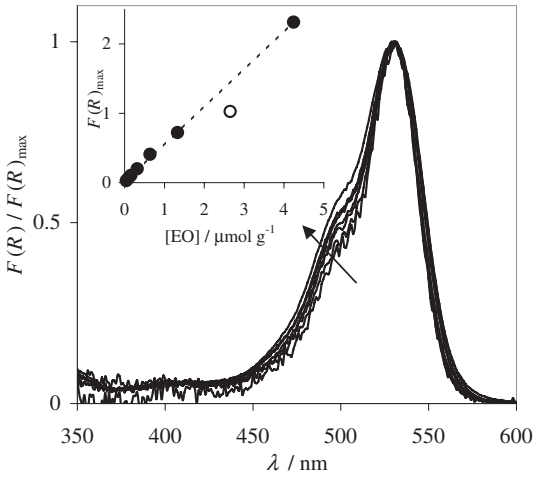

Figure 1. Normalized remission function spectra of samples EO1–EO8. The arrow points in direction of increasing concentration. Inset: remission function at the maximum (531 nm) as a function of dye concentration. The open symbol corresponds to sample EO7. The cellulose background has been subtracted in all cases.

Fluorescence spectra and quantum yields

Normalized steady-state fluorescence spectra for optically thick samples and thin layers of particles are shown in Fig. 2. Typical effects of light reabsorption, namely redshift and growing of the shoulder at longer wavelengths, resulting from the strong absorption of the dye below 550 nm, are seen on thick layer spectra. Although strongly reduced, the same effects are observed at the highest concentrations in thin layer spectra, showing that reabsorption is not negligible also in this case. At the lowest concentrations, the shape of thin layer spectra becomes constant, but a redshift with concentration remains. This effect, not attributable to reabsorption, is typical in this kind of system and reflects again the occurrence of weak interactions between singlet excited state molecules and neighboring ground state partners (11).

Absolute fluorescence quantum yields calculated between 500 and 540 nm were corrected for reabsorption and reemission of fluorescence (23,27), leading to the true fluorescence quantum yields, Φ_F, shown in Fig. 3. A nearly constant value, $\Phi_F = 0.60 \pm 0.10$, is obtained up to 0.636 μmol g^{-1}, similar to the quantum yield found for EO in ethanol (16). At the highest loadings, concentration quenching is observed, although the aggregation tendency should be small as pointed out above. Similar results obtained for rhodamine 6G on

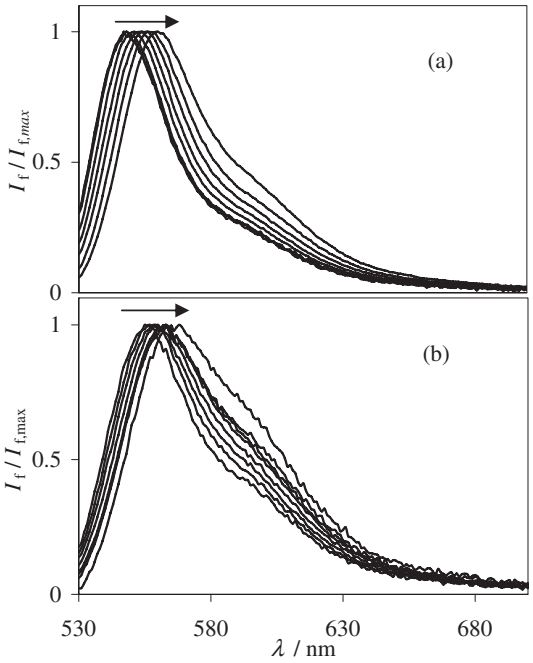

Figure 2. Normalized fluorescence spectra of (a) thin layers and (b) thick layers of samples EO1–EO8. Arrows point in direction of increasing concentration. Excitation wavelength: 500 nm.

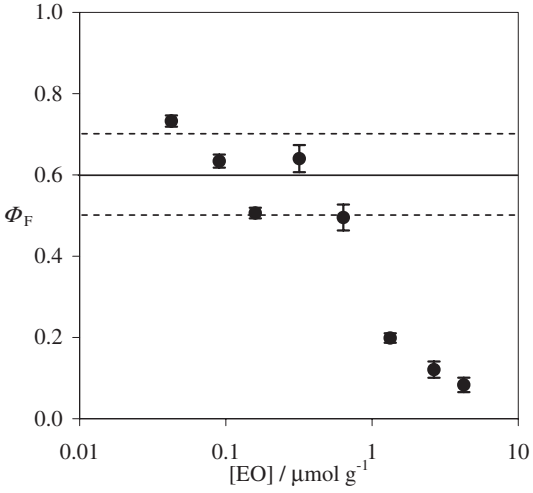

Figure 3. Fluorescence quantum yields corrected for reabsorption and re-emission as a function of dye concentration. Excitation interval: 500–540 nm.

cellulose, a system for which no aggregation could be detected spectroscopically, were attributed to excitation energy transfer and trapping (10).

Room-temperature laser induced luminescence

Time-resolved luminescence spectra in the μs-ms range are shown in Fig. 4. As pointed out above, we used the pulse of a nitrogen laser at 337 nm (600 ps half width) as excitation source, thus avoiding deconvolution problems in the decay analysis. Spectra presented in the figure were obtained with air equilibrated samples at room temperature (20 ± 1°C). Spectra

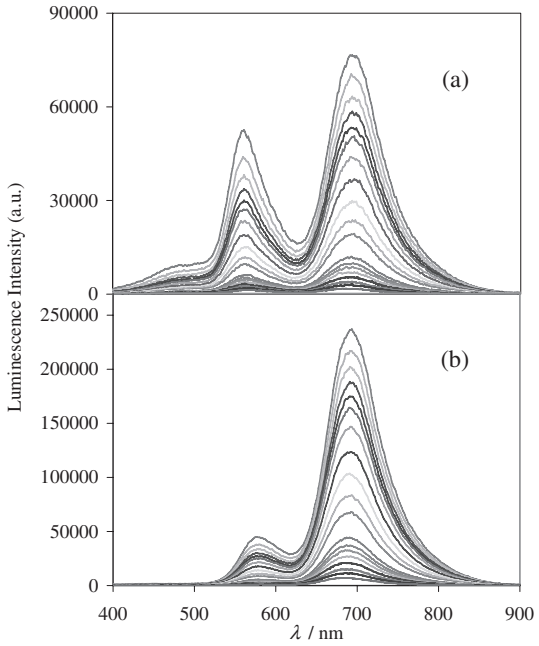

Figure 4. Time-resolved luminescence spectra of eosin Y adsorbed on microcrystalline cellulose for (a) 0.09 (sample EO2) and (b) 4.24 (sample EO8) μmol eosin (g cellulose)$^{-1}$ excited at 337 nm. The uppermost spectrum in each graph was obtained 100 μs after the laser pulse, following downwards up to 10 ms.

recorded for argon purged samples were identical within the experimental error, both in spectral and kinetic terms. As observed earlier (20), cellulose efficiently protects the triplet excited state of eosin from oxygen quenching.

The long-lived emission is separated into three distinct bands. The one at around 700 nm corresponds to phosphorescence from eosin Y and the band centered at about 560–570 nm to delayed fluorescence, as its spectrum resembles those of Fig. 2. At low loadings, some emission from cellulose can be observed at the blue side of the spectrum (35), which is strongly reduced at high loadings. This emission is particularly important at low-dye loadings (*e.g.* for sample EO2) because cellulose absorption is large at the excitation wavelength, whereas the efficiency of delayed fluorescence (not measured) is in general quite low. At higher loadings, the fraction of light absorbed by cellulose is much smaller and reabsorption of its emission by the dye increases, so that no cellulose emission is observed for sample EO8.

Phosphorescence spectra are independent of the concentration of the dye and shift to shorter wavelengths as time evolves, whereas keeping their shape, as shown in Fig. 5 for sample EO8. Phosphorescence decays are complex, consistent with the heterogeneous environment currently found in polymers, but independent of concentration as well. These facts can be rationalized as follows. The exciton interaction between a pair of dye molecules depends on the dipole moment of the radiative transition carrying the monomer from the ground to the excited state, being thus dependent on the multiplicity of the excited pair. Even for a weakly interacting singlet pair, nonradiative decay to the ground and triplet state may be enhanced with none or slight fluorescence emission (36), leading to a concentration dependent fluorescence quantum yields as shown in Fig. 3. On the other hand,

triplet pairs, showing negligible interaction, decay in the same way as the monomer; thus triplet decays are concentration independent.

As shown in Fig. 6, LDA yields a bimodal lifetime distribution, α, with maxima peaking at *ca* 750 and 3000 μs for sample EO8. The distribution at shorter lifetimes is broader than that found at longer lifetimes. The same behavior is obtained for all samples. Lifetimes are in the order of those found in the literature for room-temperature phosphorescence of eosin Y in different rigid matrices, although in most cases single lifetimes are reported (37–40). Lettinga *et al*. (38) have found a value around 4 ms for the phosphorescence lifetime of eosin Y in polyvinyl alcohol films, in the order of the longer lifetime distribution found in cellulose. Lam *et al*. (40) observed a lifetime of 2.96 ms for the same dye in gelatin, but a shorter phosphorescence lifetime in sol–gel silica, 0.76 ms. This shorter lifetime was attributed in that case to oxygen quenching due to the permeability of the silica matrix to oxygen compared with gelatin. Even when it is in the order of the shorter distribution lifetime found in cellulose, in our case this component cannot be assigned to oxygen quenching (see above). As spectra shift to the blue with time, the slow decaying component has to be associated with a triplet characterized by a higher energy.

According to the lifetimes of the fast and slow components shown in Fig. 6, it can be ascertained that only the slow decaying triplet will be present at 10 ms. Therefore, the spectrum at this time can be attributed to the higher energy triplet. In contrast, the spectrum of the faster decaying triplet is unknown because both kinds of triplets are present at the beginning of the experiment. To obtain the unknown spectrum bilinear analysis was performed (see the Materials and Methods section). Analysis of spectra shown in Fig. 4 at $\lambda > 650$ nm shows that emission can be formally decomposed with excellent confidence into two components decaying nonexponentially, each one corresponding to a different triplet species. The spectrum of the faster decaying triplet is one of the infinite linear combinations, which may be obtained subtracting the spectrum at $t = 10$ ms (slow decaying triplet) from the initial spectrum (both components). Spectra and decays shown in Fig. 7, obtained in this way, are consistent with LDA results, *i.e*. decays a and b correspond nearly to the slow and the fast modes shown in Fig. 6, respectively.

The luminescence lifetime distribution allows estimating the relative abundances of both kinds of triplets, as the area below each mode in the distribution α *vs* ln τ is proportional to the number of excited molecules emitting within each environment (41). For EO8 (see Fig. 6), LDA provides two Gaussian distributions whose maxima are 89 and 296 (in arbitrary units) and have FWHM values of 2.54 and 0.84, for the short and long-lived triplets, respectively. The area ratio is thus 0.92 and the fractions of both components are therefore 0.48 and 0.52, respectively. In Fig. 7, both spectra were adjusted to the same amplitude assuming equal oscillator strengths. After this adjustment, almost equal abundances are obtained at $t = 0$ (see lower panel in the figure), consistently with LDA results.

Figure 8 shows delayed fluorescence spectra taken at 100 μs for all samples, normalized at the phosphorescence maxima. In

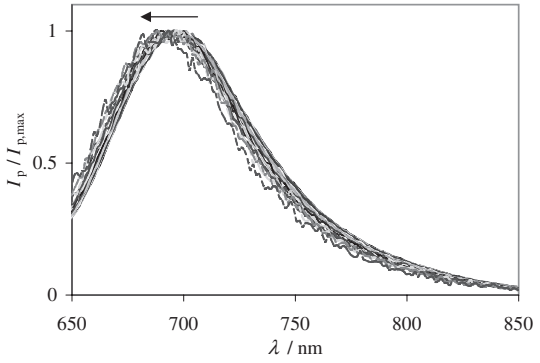

Figure 5. Shift of the phosphorescence spectrum observed for sample EO8 from $t = 100$ μs to 10 ms in the direction of the arrow.

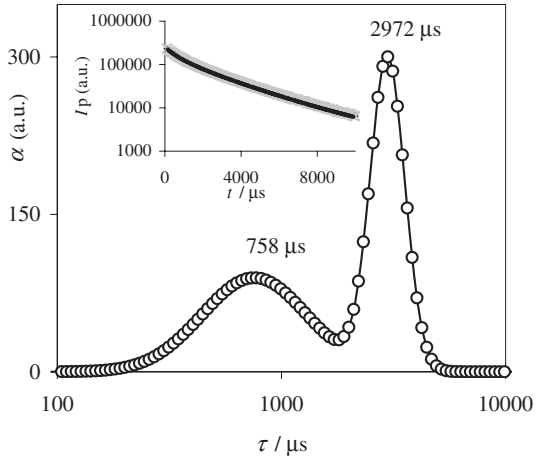

Figure 6. Lifetime distribution analysis for sample EO8 phosphorescence. Inset: experimental (full line) and calculated (*x*) decays.

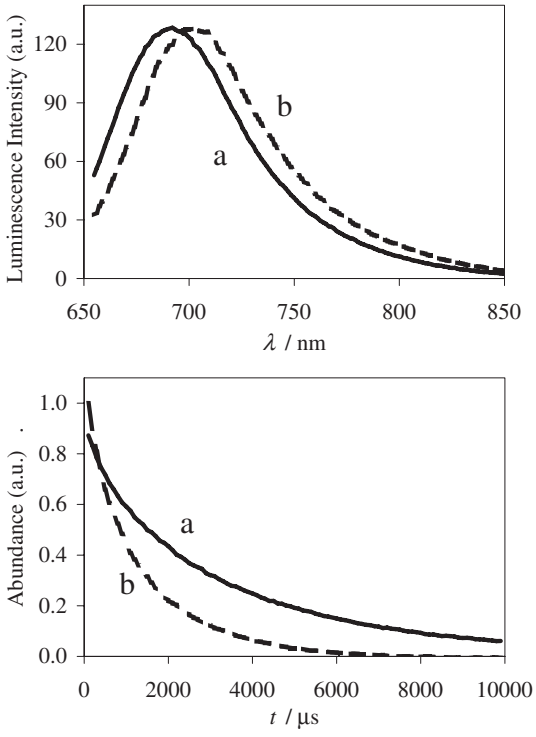

Figure 7. Phosphorescence spectra and decays obtained for sample EO8 by bilinear analysis (see text); a and b are the slower and faster decaying components, respectively.

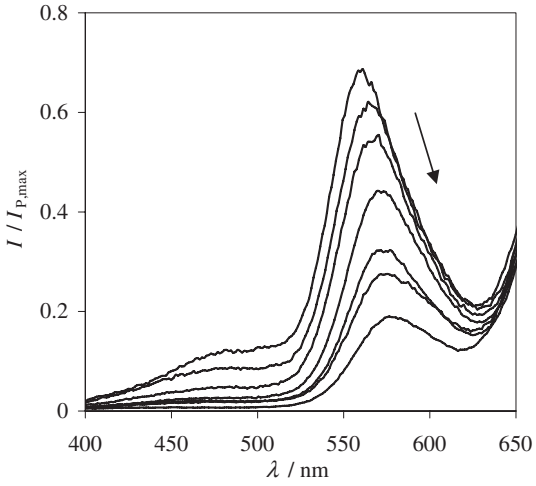

Figure 8. Delayed fluorescence spectra at 100 μs after the laser pulse for samples EO2–EO8 normalized at the phosphorescence maxima. The arrow points in the direction of increasing concentration.

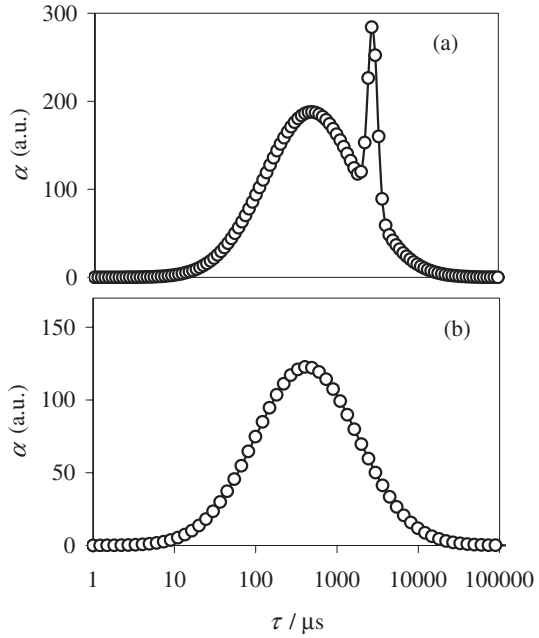

Figure 9. Lifetime distribution analysis of (a) delayed fluorescence of sample EO3 and (b) luminescence of the support (microcrystalline cellulose).

contrast to phosphorescence spectra, delayed fluorescence spectra depend on the concentration of the sample, but remain essentially constant during the whole decay.

Phosphorescence spectra are almost not contaminated by any other emission above 650 nm. In contrast, delayed fluorescence spectra are superimposed at the red side with the phosphorescence tail and, at the blue side, with emission from cellulose. Reabsorption effects are responsible for the observed redshift and the decrease of relative emission intensities as dye concentration increases. On the other hand, the lifetime distribution is modified by the presence of cellulose emission because its spectrum, peaking at 530 nm, overlaps with delayed fluorescence. As absorption of eosin Y has also its maximum near 530 nm, strong reabsorption takes place mainly at the largest concentrations and part of the cellulose emission is converted into eosin fluorescence, decaying with the typical lifetime distribution of cellulose. As a result of reverse intersystem crossing and energy transfer from cellulose, a trimodal lifetime distribution is expected for delayed fluorescence decays.

However, Fig. 9 shows a bimodal distribution for sample EO3. Bands are centered at approximately the same lifetimes as for phosphorescence, but the band at shorter lifetimes is much broader and similar to that observed for pure cellulose. Therefore, the last band can be attributed to fluorescence arising from reabsorption of cellulose emission. A small contribution from delayed fluorescence arising from fast decaying triplets, not resolved by LDA, might also be present. The band at longer lifetimes is in the same location and has the same width as the corresponding band shown for sample EO8 in Fig. 6 (recall that phosphorescence decays are independent of dye concentration).

Results indicate that eosin Y triplets are distributed into two different environments. One of them is highly ordered, the dye being well entrapped into the cellulose polymer chains, previously swelled by the use of a protic and polar solvent as ethanol (21). In this environment, eosin exhibits the largest phosphorescence lifetime due to the high constraint imposed by entrapment, resulting in the decrease of nonradiative deactivation pathways. The distribution at shorter lifetimes, showing the largest width, is assigned to eosin located in more disorganized, *i.e.* amorphous regions of cellulose. In this environment, adsorption sites are characterized by stronger interactions with stereochemically available cellulose hydroxyl groups, lowering the triplet energy and enhancing radiationless deactivation.

Pastukhov *et al.* (42) and Barinov *et al.* (43) found similar results for eosin Y in low-temperature glycerol–water glasses. At 130 K for a 66% water–glycerol solution, a blueshift of the phosphorescence spectrum with time in the ms range was attributed to static inhomogeneous broadening (site heterogeneity). A higher nonradiative deactivation rate of the dye at the long-wavelength side of the phosphorescence band was also observed. It has to be recalled that the last result, obtained following the decay at a fixed wavelength, is surely distorted by the progressive shift of the spectrum with time. This effect is less notorious when decays are analyzed near the maximum of the phosphorescence band, as it was carried out in this study. However, at temperatures between 160–200 K (near the glass transition temperature), the same authors report a shift of the phosphorescence spectrum to lower energies, attributed to orientational relaxation of the water–glycerol mixture around the excited chromophore. Quite similar effects as those found here were encountered by Pravinata *et al.* in their study on erythrosin B on amorphous sucrose (19), namely a blueshift in phosphorescence with time and a shorter lifetime for less-energetic triplets. The temperature range was around the glass transition temperature of amorphous sucrose, 65°C. Triplet decays follow in this case stretched exponentials. Results are consistent with spatial and temporal heterogeneity, the last resulting from solvation dynamics in the time range of the triplet decay.

Laser induced luminescence at 77 K

To evaluate the possible role of dynamic heterogeneity in our case, measurements at low temperature (77 K) were

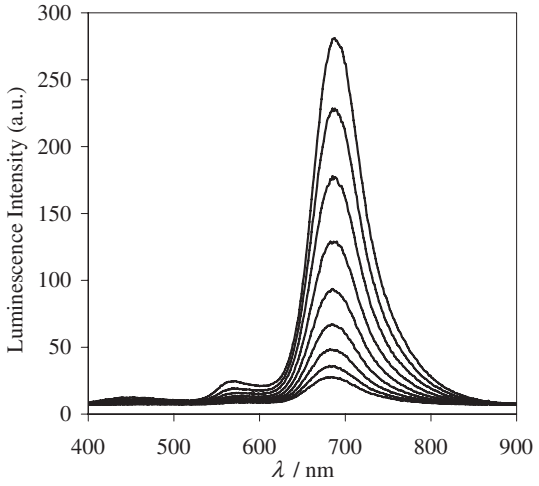

Figure 10. Time-resolved luminescence spectra at 77 K for sample EO8 (4.24 μmol g^{-1}) excited at 337 nm. The uppermost spectrum was obtained 100 μs after the laser pulse, following downwards in 1000 μs steps.

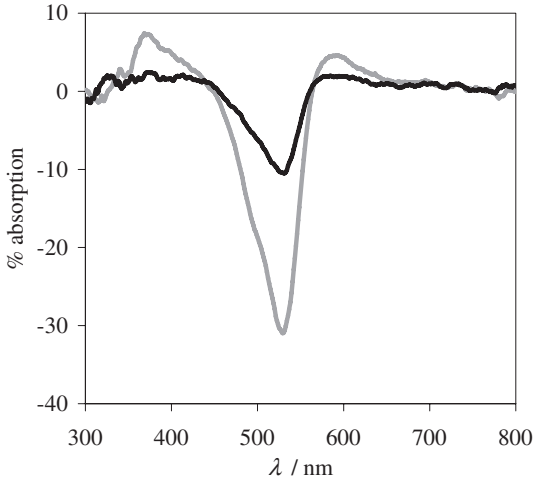

Figure 11. Transient absorption spectrum of eosin Y adsorbed onto microcrystalline cellulose, air equilibrated, recorded immediately (gray line) and 5 ms after (black line) the laser pulse. The guest concentration was 0.64 μmol g^{-1} (sample EO5).

performed. Figure 10 shows time-resolved luminescence spectra taken at this temperature for sample EO8. The same behavior as observed at room temperature (Fig. 4b) is found for the long-wavelength band, *i.e.* decay in the ms domain and blueshift of the emission spectrum with time. Comparison between the delayed fluorescence spectra obtained at room temperature and the low-temperature emission, shows that delayed emission is almost absent in the latter case. Back intersystem crossing is strongly reduced at 77 K. There is still some emission peaking at about 570 nm, derived from reabsorption of cellulose emission.

It is interesting to note that room temperature and 77 K phosphorescence emission of eosin Y decays with very similar rates, showing again the importance of the rigid environment due to cellulose entrapment. This result shows that relaxation of the cellulose subsystem responsible for enhanced radiationless deactivation of the triplet state should take place faster than triplet decay at both temperatures. This implies in turn that there is essentially no reorganization of the medium within the triplet timescale.

The glass transition temperature in the amorphous regions of dry microcrystalline cellulose is supposed to be at least 133°C, although other transition ranges at higher temperature have been found (44). Therefore, dynamic effects should be minimal at room temperature, perhaps restricted to the motion of hydroxyl groups within the cellulose chains. According to the preparation method, the dye remains entrapped after solvent evaporation and amorphous regions in the cellulose matrix become frozen, the main difference with crystalline regions regarding interaction with the dye being the capability of extensive hydrogen bonding.

DRLFP

Time-resolved absorption spectra were obtained by DRLFP. The use of an ICCD detector allowed us to obtain time-resolved absorption spectra with nanometer spectral spacing in the 250–950 nm range. No significative changes in spectral shape are detected between the transient absorption recorded immediately after the laser pulse and 5 ms later (see Fig. 11). The timescale is compatible with the phosphorescence lifetime distributions obtained from the LIL studies, showing that we are observing indeed the transient absorption of the triplet excited state of eosin Y.

CONCLUSIONS

Weak exciton interactions between the excited singlet state and ground state molecules are responsible for changes in the absorption spectra, the redshift in fluorescence spectra (once corrected for reabsorption effects) and fluorescence quenching through energy trapping on increasing the dye concentration. In contrast, the dye triplet state is not sensitive to changes in concentration. Thus, it decays in the same way within the whole concentration range.

Spectroscopic data show that the eosin Y triplet state is sensitive to the molecular environment. Eosin adsorbed in more amorphous regions shows lower triplet lifetimes and emission occurs from more stabilized triplets (redshifted phosphorescence). The opposite behavior is found in the more rigid (crystalline) environment. As time increases, the triplet population is enriched in more energetic, long-lived triplet states, leading to the blueshift found in phosphorescence spectra as time evolves.

The dye in less-constrained regions interacts strongly with cellulose hydroxyl groups, leading to lower triplet energies and shorter lifetimes than in more ordered regions. In principle, this effect can be ascribed to differences in the dipolar relaxation of hydroxyl groups (45). The extent of interactions of the dye with cellulose hydroxyl groups due to hydrogen bonding may be the cause of found differences in triplet energies and lifetimes in different regions of the support, as those interactions stabilize the triplet state and facilitate nonradiative deactivation of the excited state through dissipation of vibrational energy into the matrix, leading to shorter lifetimes (19).

Further studies are being undertaken to elucidate the exact role of dye-to-support interactions on the photophysics of the triplet state. Found effects are similar to those encountered in

amorphous systems, but rather than being assigned to a change in the environment during the triplet lifetime, in our case they are ascribed to spatial heterogeneity because similar time-dependent blueshifts and phosphorescence lifetimes were observed at low temperature (77 K). Phosphorescence and delayed fluorescence could be measured at room temperature and at 77 K without degassing because the cellulose environment protects the triplet state from oxygen quenching.

Acknowledgements—This work was supported by the CONICET (PIP 0319), ANPCyT (PICT 00938) and UBA (UBACyT X202). E. S. R. is a staff member of CONICET. H. B. R. acknowledges CONICET for a postdoctoral fellowship. Many thanks are due to Pedro Aramendía for enlightening discussion. L. F. V. F., P. D. and I. F. M thank FCT for financial support (Project PTDC/QUI/65510/2006 and PTDC/QUI/70153/2006). E. S. R. and L. F. V. F. acknowledge a grant from the MINCyT-FCT program project PO/09/32.

REFERENCES

1. Shirke, S. and R. D. Ludescher (2005) Dynamic site heterogeneity in amorphous maltose and maltitol from spectral heterogeneity in erythrosin B phosphorescence. *Carbohydr. Res.* **340**, 2661–2669.
2. Lukasik, K. V. and R. D. Ludescher (2006) Effect of plasticizer on dynamic site heterogeneity in cold-cast gelatin films. *Food Hydrocoll.* **20**, 88–95.
3. Tomczak, N., R. A. L. Vallée, E. M. H. P. van Dijk, M. García-Parajó, L. Kuipers, N. F. van Hulst and G. J. Vancso (2004) Probing polymers with single fluorescent molecules. *Eur. Polym. J.* **40**, 1001–1011.
4. Wagner, B. D. (2009) The use of coumarins as environmentally-sensitive fluorescent probes of heterogeneous inclusion systems. *Molecules* **14**, 210–237.
5. Mishra, A., M. K. R. Fisher and P. Bäuerle (2009) Metal-free organic dyes for dye-sensitized solar cells: from structure:property relationships to design rules. *Angew. Chem. Int. Ed.* **48**, 2474–2499.
6. Hagfeldt, A., G. Boschloo, L. Sun, L. Kloo and H. Pettersson (2010) Dye-sensitized solar cells. *Chem. Rev.* **110**, 6595–6663.
7. Bechet, D., P. Couleaud, C. Frochot, M.-L. Viriot, F. Guillemin and M. Barberi-Heyoh (2008) Nanoparticles as vehicles for delivery of photodynamic therapy agents. *Trends Biotechnol.* **26**, 612–621.
8. Brewer, S. A., C. Perdomo Artiles, J. A. Taylor and M. Dennis (2010) Photosensitive dyes and self-detoxifying textiles: degradation products and dye durability. *Appl. Surf. Sci.* **256**, 1908–1912.
9. Kasha, M., H. R. Rawls and M. A. El-Bayoumi (1965) The exciton model in molecular spectroscopy. *Pure Appl. Chem.* **11**, 371–392.
10. López, S. G., G. Worringer, H. B. Rodríguez and E. San Román (2010) Trapping of Rhodamine 6G excitation energy on cellulose microparticles. *Phys. Chem. Chem. Phys.* **12**, 2246–2253.
11. Rodríguez, H. B. and E. San Román (2008) Excitation energy transfer and trapping in dye-loaded solid particles. *Ann. N.Y. Acad. Sci.* **1130**, 247–252.
12. Blossey, E. C., D. C. Neckers, A. L. Thayer and A. P. Schaap (1973) Polymer-based sensitizers for photooxidations. *J. Am. Chem. Soc.* **95**, 5820–5822.
13. Hawn, D. D. and N. R. Armstrong (1978) Electrochemical adsorption and covalent attachment of erythrosin to modified tin dioxide electrodes and measurement of the photocurrent sensitization to visible wavelength light. *Phys. Chem.*, **82**, 1288–1295.
14. Fleming, G. R., A. W. E. Knight, J. M. Morris, R. J. S. Morrison and G. W. Robinson (1977) Picosecond fluorescence studies of xanthene dyes. *J. Am. Chem. Soc.* **99**, 4306–4311.
15. Reindl, S. and A. Penzkofer (1996) Triplet quantum yield determination by picosecond laser double-pulse fluorescence excitation. *Chem. Phys.* **213**, 429–438.
16. Seybold, P. G., M. Gouterman and J. Callis (1969) Calorimetric, photometric and lifetime determinations of fluorescence yields of fluorescein dyes. *Photochem. Photobiol.* **9**, 229–242.
17. Penzkofer, A., A. Beidoun and M. Daiber (1992) Intersystem-crossing and excited-state absorption in eosin Y solutions determined by picosecond double pulse transient absorption measurements. *J. Lumin.* **51**, 297–314.
18. Penzkofer, A., A. Tyagi, E. Slyusareva and A. Sizykh (2010) Phosphorescence and delayed fluorescence properties of fluorone dyes in bio-related films. *Chem. Phys.* **378**, 58–65.
19. Pravinata, L. C., Y. You and R. D. Ludescher (2005) Erythrosin B phosphorescence monitors molecular mobility and dynamic site heterogeneity in amorphous sucrose. *Biophys. J .* **88**, 3551–3561.
20. Wilkinson, F., P. A. Leicester, L. F. Vieira Ferreira and V. M. M. R. Freira (1991) Photochemistry on surfaces: triplet-triplet energy transfer on microcrystalline cellulose studied by diffuse reflectance transient absorption and emission spectroscopy. *Photochem. Photobiol.* **54**, 599–608.
21. Vieira Ferreira, L. F., J. C. Netto-Ferreira, I. V. Khmelinskii, A. R. Garcia and S. M. B. Costa (1995) Photochemistry on surfaces: matrix isolation mechanisms study of interactions of benzophenone adsorbed on microcrystalline cellulose investigated by diffuse reflectance and luminescence techniques. *Langmuir* **11**, 231–236.
22. Vieira Ferreira, L. F., A. R. Garcia, M. R. Freixo and S. M. B. Costa (1993) Photochemistry on surfaces: solvent–matrix effect on the swelling of cellulose. An emission and absorption study of adsorbed auramine O. *J. Chem. Soc., Faraday Trans.* **89**, 1937–1944.
23. Rodríguez, H. B., M. G. Lagorio and E. San Román (2004) Rose Bengal adsorbed on microgranular cellulose: evidence on fluorescent dimers. *Photochem. Photobiol. Sci.* **3**, 674–680.
24. Rodríguez, H. B. and E. San Román (2007) Energy transfer from chemically attached rhodamine 101 to adsorbed methylene blue on microcrystalline cellulose particles. *Photochem. Photobiol.* **83**, 547–555.
25. Wendlandt, W. W. and H. G. Hecht (1966) *Reflectance Spectroscopy*, Ch. 3, pp. 55–76. Wiley Interscience, New York, NY.
26. Vieira Ferreira, L. F., M. R. Freixo, A. R. Garcia and F. Wilkinson (1992) Photochemistry on surfaces: fluorescence emission quantum yield evaluation of dyes adsorbed on microcrystalline cellulose. *J. Chem. Soc., Faraday Trans.* **88**, 15–22.
27. Lagorio, M. G., L. E. Dicelio, M. I. Litter and E. San Roman (1998) Modeling of fluorescence quantum yields of supported dyes. Aluminium carboxyphthalocyanine on cellulose. *J. Chem. Soc., Faraday Trans.* **94**, 419–425.
28. Mirenda, M., M. G. Lagorio and E. San Román (2004) Photophysics on surfaces: determination of absolute fluorescence quantum yields from reflectance spectra. *Langmuir* **20**, 3690–3697.
29. Vieira Ferreira, L. F., T. J. F. Branco and A. M. Botelho do Rego (2004) Luminescence quantum yield determination for molecules adsorbed onto solid powdered particles. *Chem. Phys. Chem.* **5**, 1848–1854.
30. Vieira Ferreira, L. F. and I. L. Ferreira Machado (2007) Surface photochemistry: organic molecules within nanocavities of calixarenes. *Curr. Drug Discov. Technol.* **4**, 229–245.
31. Branco, T. J. F., A. M. Botelho do Rego, I. Ferreira Machado and L. F. Vieira Ferreira (2005) Luminescence lifetime distributions analysis in heterogeneous systems by the use of excel's solver. *J. Phys. Chem. B* **109**, 15958–15967.
32. San Román, E. and M. C. González (1989) Analysis of spectrally resolved kinetic data and time-resolved spectra by bilinear regression. *J. Phys. Chem.* **93**, 3532–3536.
33. Wilkinson, F. and P. G. Kelly (1989) Diffuse reflectance flash-photolysis. In *Handbook of Organic Photochemistry*, Vol. 1, Ch. 12 (Edited by J. C. Scaiano), pp. 293–315. CRC Press, Boca Raton, FL.
34. Botelho do Rego, A. M. and L. F. Vieira Ferreira (2001) Photonic and electronic spectroscopies for the characterization of organic surfaces and organic molecules adsorbed on surfaces. In *Handbook of Surfaces and Interfaces of Materials*, Vol. 2, Ch. 7 (Edited by H. S. Nalwa), pp. 275–313. Academic Press, New York, NY.
35. McAleese, D. L. and R. B. Dunlap (1984) Reduction of background emission in room-temperature phosphorescence. *Anal. Chem.* **56**, 600–601.
36. McRae, E. G. and M. Kasha (1958) Enhancement of phosphorescence ability upon aggregation of dye molecules. *J. Chem. Phys.* **28**, 721–722.

37. Lindvold, L. R., A. R. Beierholm and C. E. Andersen (2010) An organic dye in a polymer matrix—a search for a scintillator with long luminescent lifetime. *Radiat. Meas.* **45**, 615–617.
38. Lettinga, M. P., H. Zuilhof and M. A. M. J. van Zandvoort (2000) Phosphorescence and fluorescence characterization of fluorescein derivatives immobilized in various polymer matrices. *Phys. Chem. Chem. Phys.* **2**, 3697–3707.
39. Lettinga, M. P., M. A. M. J. van Zandvoort, C. M. van Kats and A. P. Philipse (2000) Phosphorescent colloidal silica spheres as tracers for rotational diffusion studies. *Langmuir* **16**, 6156–6165.
40. Lam, S. K. and D. Lo (1997) Time-resolved spectroscopic study of phosphorescence and delayed fluorescence of dyes in silica-gel glasses. *Chem. Phys. Lett.* **281**, 35–43.
41. Ferreira Machado, I. L., L. F. Vieira Ferreira and A. S. Oliveira (2010) Luminescence and diffuse reflectance studies of biacetyl included within *p*-tert-butylcalixarenes. *J. Lumin.* **130**, 2251–2255.
42. Pastukhov, A. V., D. V. Khudyakov, V. R. Vogel and A. I. Kotelnikov (2001) A supercooled glycerol–water mixture: evidence for the large-scale heterogeneity? *Chem. Phys. Lett.* **346**, 61–68.
43. Barinov, A. B., N. S. Goryachev and A. I. Kotelnikov (2011) Analysis of microsecond relaxation dynamics of proteins and viscous media by recording relaxation shifts of phosphorescence spectra. *Optics Spectr.* **110**, 724–729.
44. Sun, C. C. (2008) Mechanism of moisture induced variations in true density and compaction properties of microcrystalline cellulose. *Int. J. Pharm.* **346**, 93–101.
45. Richert, R. (2000) Triplet state solvation dynamics: basics and applications. *J. Chem. Phys.* **113**, 8404–8429.